PCCP

ROYAL SOCIETY OF CHEMISTRY

PAPER

View Article Online
View Journal | View Issue

Cite this: *Phys. Chem. Chem. Phys.*, 2025, **27**, 16195

Alkali metal cation-anchored hydrated hydroxide complexes at the nanoscale interface as catalytic active sites for selective liquid-phase aerobic oxidation of benzyl alcohol to benzaldehyde†

Bo Peng,[ab] Weiyu Zhou,[ab] Jiayu Dong,[ab] Changjiu Xia,*[c] Peng Wu[abd] and Kun Zhang*[abd]

Although water and alkali species synergistically activate C–H bonds and O_2 molecules in alcohol selective oxidation, the chemical states of these species and their regulatory mechanisms of the reaction pathways remain poorly understood. Herein, we report that alkali metal hydroxides alone act as efficient catalysts for the selective oxidation of benzyl alcohol to benzaldehyde under aqueous conditions. The catalytic efficiency is profoundly governed by the microstructural interplay at the biphasic interface, which is delicately modulated by parameters including the type and dosage of base, water content, alkali cation identity, and solvent polarity. Through isotopic labeling experiments and advanced spectroscopic analyses—including UV-vis absorption, fluorescence spectroscopy, and ^{1}H NMR—we identify the active catalytic site as a hydrated hydroxide complex anchored by alkali metal cations at the biphasic nanoheterogeneous interface. Notably, smaller alkali metal cations exhibit stronger water-binding affinity, which paradoxically reduces the reactivity for benzaldehyde formation. This counterintuitive behavior is attributed to metastable interfacial states that favor substrate and O_2 activation, thereby accelerating electron transfer and reaction kinetics. Our findings reveal that these complexes generate surface electronic states (SESs) through spatial orbital overlap between O atoms in H_2O and OH^-, enabling concerted electron–proton transfer. This work not only clarifies the pivotal role of hydrated hydroxide complexes in selective alcohol oxidation, but also provides new insights into the design of metal-free catalytic systems for sustainable chemical synthesis.

Received 21st March 2025,
Accepted 3rd July 2025

DOI: 10.1039/d5cp01109d

rsc.li/pccp

Introduction

Direct liquid-phase oxidation of alcohols using molecular oxygen represents a promising strategy in organic synthesis, offering green pathways for producing high-value chemicals and intermediates. Benzaldehyde, a versatile intermediate and high value-added fine chemical, is widely used across pharmaceuticals, dyestuffs, food, cosmetics, and agrochemical industries.[1–4] However, conventional alcohol oxidation methods often rely on stoichiometric amounts of toxic high-valent metal salts or organic oxidants, posing significant economic and environmental challenges.[5–8] Over the past two decades, noble metals (*e.g.*, Pt, Au, Pd) and transition metals have been extensively used as heterogeneous catalysts for alcohol oxidation.[9–24] Yet, their activity and selectivity typically depend on the presence of a base (usually NaOH or K_2CO_3), which facilitates O–H and C–H bond cleavage in alcohols.[17,25–32] For instance, Jiang *et al.*[33] reported that Au nanoparticles supported on various metal–organic framework (MOF) catalysts have often been documented to give relatively high yields of aldehyde formation under basic conditions in the oxidation of aqueous alcohols, but some of the catalysts show no activity in the absence of NaOH. The importance of the base was generally related to the coverage of OH on the metal surface, which can facilitate the cleavage of the O–H and C–H bonds in alcohol.[34,35] Notably, NaOH can also catalyze selective aerobic alcohol oxidation without metal catalysts,[36,37] suggesting that the base itself may play a more critical role than previously recognized. Similar to bases, water

[a] *State Key Laboratory of Petroleum Molecular & Process Engineering, School of Chemistry and Molecular Engineering, East China Normal University, Shanghai 200062, China. E-mail: kzhang@chem.ecnu.edu.cn*
[b] *Shanghai Key Laboratory of Green Chemistry and Chemical Processes, School of Chemistry and Molecular Engineering, East China Normal University, Shanghai 200062, China*
[c] *State Key Laboratory of Catalytic Materials and Reaction Engineering, Research Institute of Petroleum Processing, SINOPEC, Beijing 100083, China. E-mail: xiachangjiu.ripp@sinopec.com*
[d] *Institute of Eco-Chongming, Shanghai, China*

† Electronic supplementary information (ESI) available. See DOI: https://doi.org/10.1039/d5cp01109d

acts as a promoter in alcohol aerobic oxidation, directly participating in the reaction and enhancing kinetics. Recent studies have begun to elucidate water's role at nanoscale interfaces, but the interplay between interfacial OH^- species and water, and their influence on electron and proton transfer, remains unclear.[35,38–44]

Recent experimental and quantum mechanical studies have revealed that hydrated hydroxide complexes, also termed structural water molecules (SWs), confined within specially designed nanocavities, are responsible for bright photoluminescence in structured nanomaterials.[45–51] These SWs are not conventional hydrogen-bonded water molecules; instead, their O atoms' p-orbitals form a new p-band intermediate state (PBIS) through spatial interactions, exhibiting π-bonding characteristics,[52,53] and thus display unique electronic and optical properties.[50] This discovery resolved a century-long debate on whether and how water can emit light.[54,55] Follow-up research showed that SW-dominated surface states not only regulate the photoluminescence of metal nanoclusters but also enhance the catalytic kinetics by mediating electron and proton transfer at heterogeneous nanoscale interfaces.[53,56–64]

Inspired by the concept of SWs as both emitters and catalytic active centers, we investigated the liquid-phase oxidation of benzyl alcohol to benzaldehyde using oxygen as the oxidant in organic solvents. Our work elucidates how hydrated hydroxide complexes, mediated by alkali metal cations, accelerate synergistic proton and electron transfer in the absence of metal catalysts, thereby enhancing the reaction kinetics. We found that alkali metal hydroxides alone can efficiently catalyze this oxidation, with performance highly dependent on base dosage, water content, alkali cation type, and solvent. Notably, chemical reactivity exhibits a significant upward trend with increasing alkali metal ion radius ($Li^+ < Na^+ < K^+ < Rb^+ < Cs^+$). Through isotopic labeling and advanced spectroscopic analyses (fluorescence, and ^1H NMR), we identified the active catalytic site as an alkali metal cation-anchored hydrated hydroxide complex featuring a distinct π-bonding structure. Unlike isolated water molecules or hydroxide ions, this complex confined at the biphasic heterogeneous interface bridges the substrate and O_2 *via* spatial p-orbital interactions, thereby accelerating surface electron transfer through π conjugation and enhancing the reaction kinetics.

Results and discussion

In the absence of a metal catalyst, the conversion of benzyl alcohol (BA) and the selectivity of benzaldehyde (BAD) using different amounts of NaOH as catalyst and O_2 as oxidant are shown in Table 1. Control experiments in the absence of NaOH demonstrated negligible BA conversion (<2%), highlighting the essential role of alkaline conditions in initiating the oxidation process. With increasing dosage of NaOH from 1 to 2 equivalent to BA, the conversion of BA increased from 44.0% to 67.3% after 2 h, accompanied by the loss of selectivity of BAD from 97.0% to 75.6%, and the main by-product was benzoic acid. A further increasing dosage of NaOH (3 equiv.) in the reaction system showed a negligible difference in the conversion of BA (63.1%) but a dramatic decrease in the selectivity of BAD (47.5%), suggesting that the reaction goes through the alcohol–aldehyde–acid pathway. Monitoring of the reaction over time confirmed that aldehyde was most likely to be the reaction intermediate (Fig. 1): as the reaction time increased, the conversion of BA increased continuously from 35.6% to 98.7% within 150 minutes, while the selectivity of BAD decreased from 81.3% to 9.7%. To further understand the kinetics of the oxidation process of benzyl alcohol, the effect of reaction temperature on overall conversion and selectivity for benzaldehyde and benzoic acid was investigated (Fig. S1 and Table S1, ESI†). Both the overall conversion and benzoic acid selectivity increased with temperature, similar to the trend observed with reaction time. This further supports that oxidation of benzyl alcohol followed continuous reaction pathways, whereby benzaldehyde was first generated and then transformed into benzoic acid (Fig. 1b). Gas source screening (Table 1) confirmed that O_2 was directly involved in the reaction process as an oxidant, and only traces of BA (~3%) converted to BAD were detected under a N_2 atmosphere, probably due to incomplete replacement of O_2 by N_2.

Table 1 Effect of reaction parameters on benzyl alcohol conversion and benzaldehyde selectivity in liquid-phase oxidation[a]

Entry	NaOH (equiv.)	Atmosphere	Time (h)	Conv. (%)	Sel. (%) Benzaldehyde	Sel. (%) Benzoic acid
1	—	O_2	1	—	—	—
			2	2	>99	—
2	1	O_2	1	22.9	>99	—
			2	44.0	97.0	3.0
3	2	O_2	1	44.0	78.5	21.5
			2	67.3	75.6	24.3
4	2	N_2	1	—	—	—
			2	3	>99	—
5	3	O_2	1	41.2	70.7	29.3
			2	63.1	47.5	52.3

[a] Reaction conditions: 10 ml toluene, 100 μl benzyl alcohol, 100 μl *n*-decane (used as internal standard), 80 °C, pressure = 1 atm, O_2 bubbling rate (30 ml min^{-1}).

In the catalytic system of noble metal, the water-promoted effect on the oxidation of alcohol was frequently observed,[35,38–44] and the water absorbed on the metal surface was probably beneficial for the activation of O_2.[42,65] Interestingly, the water-promoted effect on the oxidation of BA using NaOH as a catalyst in the liquid reaction was also prominent. As shown in Fig. 2 and Table S2 (ESI†), the addition of trace amounts of water (10 μl and 20 μl) to the toluene solvent dramatically increased the conversion of BA from 44% to 83.1%. However, the addition of excess water (30–200 μl) led to a drastic reduction in benzyl alcohol (BA) conversion from 83.1% to 5.8%. This decline is likely attributed to the increased mass transfer resistance of reactants across the biphasic interface,[44,66,67] yet we cannot rule out the influence of microstructural alterations on the surface state at the oil–water

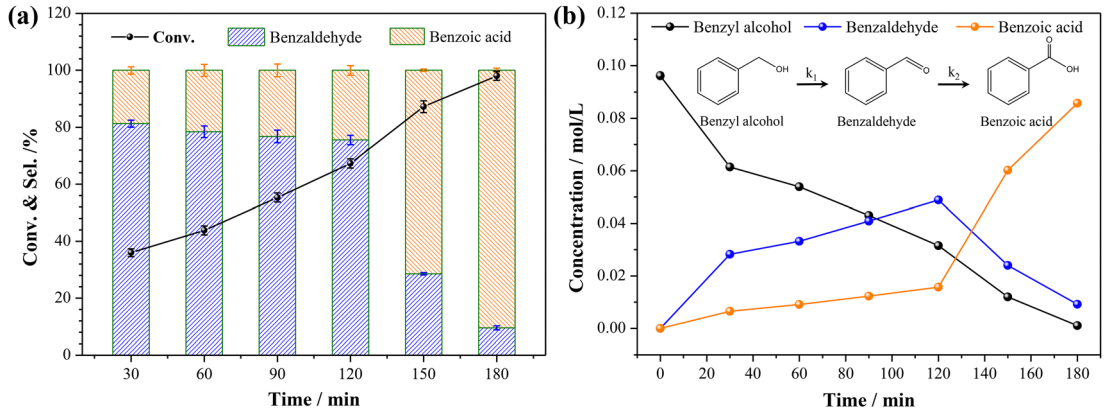

Fig. 1 Conversion/selectivity (a) and concentration (b) of the substrate and products *versus* time for the selective oxidation of benzyl alcohol using a NaOH catalyst. Reaction condition: 2 mmol NaOH, 10 ml toluene, 100 μl benzyl alcohol, 100 μl *n*-decane (used as internal standard), 80 °C, pressure = 1 atm, O_2 bubbling rate (30 ml min^{-1}). Inset: A simple kinetic model for the oxidation of benzyl alcohol. Error bars represent the standard deviations of three replicate measurements.

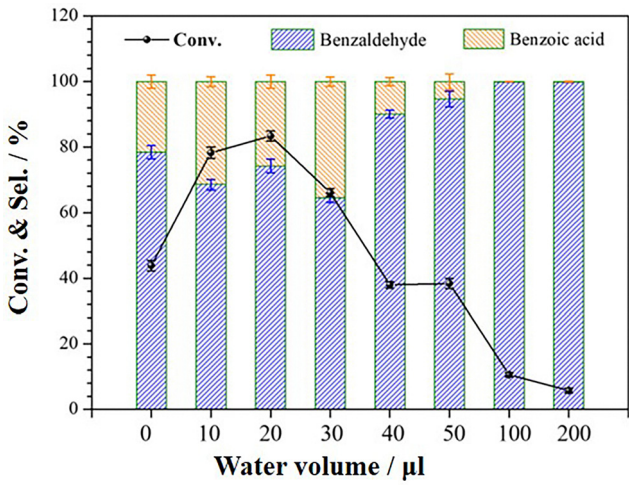

Fig. 2 Catalytic performance of NaOH catalysts with the addition of different volumes of water for the selective oxidation of benzyl alcohol. Reaction conditions: 2 mmol NaOH, 10 ml toluene, 100 μl benzyl alcohol, 100 μl *n*-decane (used as internal standard), 80 °C, pressure = 1 atm, O_2 bubbling rate (30 ml min^{-1}), time 1 h. Error bars represent the standard deviations of three replicate measurements.

interface.[68–71] The pivotal role of solvent type in modulating chemical reactivity was further corroborated by the impact of excess water on microstructural dynamics at the biphasic interface (Table S3, ESI†): high benzyl alcohol (BA) conversion was achieved in hydrophobic (nonpolar) solvents—toluene (67.3%), cyclohexane (71.9%), and *n*-heptane (>99%)—whereas negligible reactivity (Conv. <7%) was observed in hydrophilic (polar) solvents like acetonitrile, ethanol, and methanol. Therefore, the combined effects of water content and solvent polarity on catalytic performance underscore the decisive role of the biphasic heterogeneous interface in modulating chemical reactivity.

The water-promoting effect was further confirmed by the kinetic isotope effects (KIEs) using deuterated water (D_2O) instead of water (H_2O) in the same volume of water. The results of catalytic performance and reaction kinetics are shown in Fig. 3, the conversion of BA using D_2O as additives was all surpassed compared to that of H_2O at the same time no matter whether the additive volume of water was 10 μl or 50 μl (Fig. 3a and c), and all the reactions follow pseudo-first-order kinetics. The KIE (K_H/K_D) value was 0.41 and 0.82 for the addition volume of 10 and 50 μl, respectively (Fig. 3b and d), indicating that the dissociation of the O–H bond of water may not be the rate-determining step (RDS). The enhanced isotopic reaction kinetics are attributed to the stronger hydrogen bonding of heavy water relative to ordinary water molecules, which favors the stabilization of the transition state of the reaction and thus facilitates the electron and proton transfer process at the interface. These results suggest that complexes or composites composed of water and hydroxide may be catalytically active centers in the selective oxidation of benzyl alcohol and mediate the synergistic transfer of electrons and protons in the key reaction step of BA reduction to BAD, and the feature of catalytic performance is extremely sensitive to the delicate change in the surrounding micro-environment, indicating that the surface state dominated by the hydrate-hydroxide complex has meta-stability.

To further illustrate the synergistic effect of water and hydroxide, different alkali metal hydroxide catalysts were used for the selective oxidation of BA. As shown in Fig. 4a and Table S4 (ESI†), the catalytic performance of these hydroxides for the selective oxidation of BA was highly dependent on the type of alkali metal cation ($Li^+ < Na^+ < K^+ < Rb^+ < Cs^+$). LiOH catalysts showed extremely low conversion (~4.8%) of BA and thus no acid products were detected. Meanwhile, the water-promoter effect in the LiOH catalytic system was also not pronounced (Table S5, ESI†), with increasing the dosage of water volume from 0 to 100 μl, the conversion of BA was only gradually increased from 4.8% to 11.76%. The activity and the BAD selectivity of the NaOH, KOH, RbOH, and CsOH catalysts obviously showed an increasing trend from 44.0% to 100% and from 78.5% to 97.5%, respectively (Fig. 4a). In contrast to the

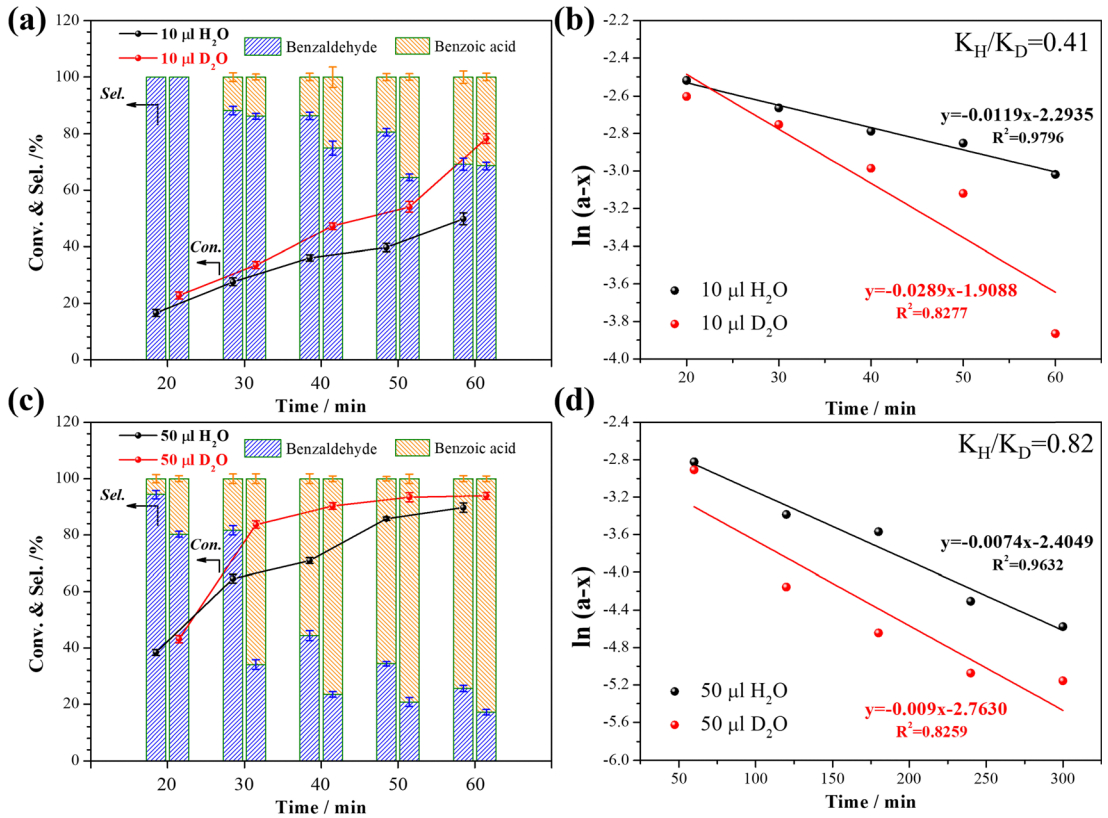

Fig. 3 Catalytic performance *versus* time (a) and (c) and reaction kinetics (b) and (d) of the NaOH catalyst with the addition of 10 μl or 50 μl H_2O and D_2O for the selective oxidation of benzyl alcohol. Reaction conditions: 2 mmol NaOH, 10 ml toluene, 100 μl benzyl alcohol, 100 μl *n*-decane (used as internal standard), 80 °C, pressure = 1 atm, O_2 bubbling rate (30 ml min^{-1}). Error bars represent the standard deviations of three replicate measurements.

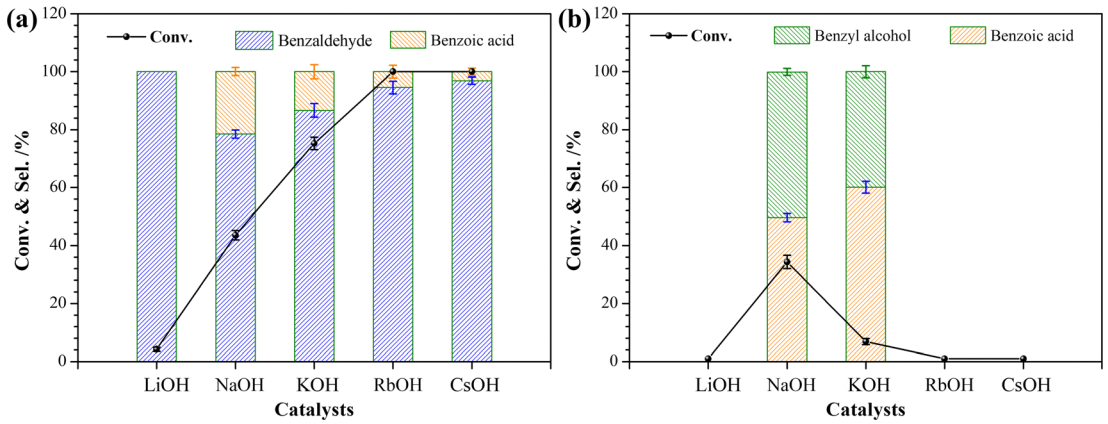

Fig. 4 Catalytic performance of MOH (M represented alkali metal cations, Li^+, Na^+, K^+, Rb^+ and Cs^+) catalysts for the selective oxidation of benzyl alcohol (a) and benzaldehyde (b). Reaction conditions: 2 mmol catalyst, 10 ml toluene, 100 μl substrate, 100 μl *n*-decane (used as internal standard), 80 °C, pressure = 1 atm, O_2 bubbling rate (30 ml min^{-1}), time 1 h. Error bars represent the standard deviations of three replicate measurements.

alcohol–aldehyde–acid reaction pathway of the NaOH catalyst, it is worth noting that the RbOH and CsOH catalysts had high activity (>99%) and high selectivity for BAD (>90%), the over-oxidation of aldehyde to acid can hardly occur with RbOH and CsOH as the catalyst, suggesting that the selectivity of BA towards BAD is strongly dependent on the nature of the alkali metal cations.

As CsOH catalysts showed the highest overall conversion and best control over benzaldehyde selectivity, we further investigated the effect of catalyst concentration (Fig. S2 and Table S6, ESI†), reaction time (Fig. S3 and Table S7, ESI†) and water additive (Fig. S4 and Table S8, ESI†) on CsOH catalytic performance. The overall conversion trend is generally similar to that of the NaOH catalytic systems (Fig. S3, ESI†), except that

the activity is insensitive to catalyst concentration (Fig. S2, ESI†), implying that a tiny amount (even as low as 0.25 mmol) of CsOH is sufficient to facilitate the oxidation of benzyl alcohol. Another prominent feature is that CsOH consistently exhibits high benzaldehyde selectivity (>99%) under various reaction conditions; however, the addition of a small amount of water (10 μl) increases the activity and generates a comparable amount of benzoic acid (Fig. S4, ESI†), suggesting kinetic control of the reaction pathways, and when the water amount was further increased to 40 μl, the chemical reactivity was almost completely quenched. This observation suggests that the surface state dominated by hydrous hydroxide complexes at the nanoscale interface is exquisitely sensitive to subtle changes in the microenvironment. Specifically, the introduction of excess water likely destabilizes the p-band intermediate state (PBIS) through hydrogen-bond interactions of water surrounding the active sites.

But, we can't completely exclude the contribution of the Cannizzaro reaction to the selectivity, where BAD could be converted to equivalent BA and benzoic acid products by a disproportionation reaction of an aldehyde lacking a hydrogen atom in the α-position to the carbonyl group.[72] As evidence, benzaldehyde was used as the substrate under the standard conditions (Fig. 4b and Table S9, ESI†), and only NaOH and KOH promote the oxidation of benzaldehyde in the absence of O_2, but showing a low BAD conversion of 33.9% and 5.8% respectively, and almost equivalent BA and benzoic acid products were obtained as expected for the Cannizzaro reaction. Therefore, in the cases of NaOH and KOH, the decline in selectivity towards BAD can be partially ascribed to the occurrence of the Cannizzaro reaction. LiOH, RbOH and CsOH catalysts showed no activity, suggesting an alkali metal cation-mediated reaction pathway for the selective oxidation of BA. To our surprise, not only the oxidation of BA but also the Cannizzaro reaction of BAD exhibit an alkali-metal cation-dependent effect. Although the investigation of the Cannizzaro reaction lies outside the scope of this research, we tentatively attribute the alkali-metal cation-dependent chemical reactivity of this reaction to hydrous hydroxide-mediated electron–proton transfer pathways. Furthermore, no activity towards BA oxidation was observed in a diagnostic experiment using alkali metal chloride as a catalyst (not shown). These results further confirmed that the active site of the hydroxide catalysts may be composed of H_2O, OH^- and M^+ (M^+ represents the alkali metal cations) in the form of $(H_2O{\cdot}OH^-)M^+$. M^+ with different atomic radius show different affinity towards H_2O and OH^-, and thus the corresponding hydroxide catalysts (MOH) showed a significant difference in reaction activity.

The chemical and electronic structure of the catalytically active centers composed of three elements (M^+, H_2O and OH^-) were further investigated using spectroscopic techniques. Fig. 5 shows the excitation and photoemission spectra of the catalytic reaction system (a mixture of toluene, BA and MOH). In contrast to the catalytic activity, the LiOH catalytic reaction system emitted the strongest fluorescence centered at *ca.* 340 nm with an excitation band at *ca.* 290 nm, which is followed by NaOH, KOH, RbOH and CsOH. The emission band centered at 340 nm was attributed to the structural water molecules confined in the hydrophobic toluene solvent according to the previously reported results.[45,46] The trend of the fluorescence intensity as a function of the affinity of the alkali metal cations for water, in the order $Li^+ > Na^+ > K^+ > Rb^+ > Cs^+$, suggests that alkali metal ions with highly bound water are more favorable for stabilizing the interfacial states formed by structural water molecules and less favorable for activating reaction substrates and molecular oxygen (Fig. 5b). However, in the absence of BA reactants, the intensity of photoluminescence (PL) did not show an alkali metal cation-dependent effect (Fig. S5, ESI†), suggesting that even at room temperature (non-reaction temperature), the introduction of BA can significantly affect the electronic structure of the surface states. Apparently, Cs^+ favors the adsorption and activation of the BA substrate, thus enhancing the reaction kinetics. A possible mechanism (Fig. 5b) was proposed to understand the catalytic process using MOH as a typical catalyst. First, the deprotonation of the OH group of BA could be achieved by interacting with an equivalent MOH and forming an alkoxide and an equivalent H_2O. And then another equivalent of MOH could

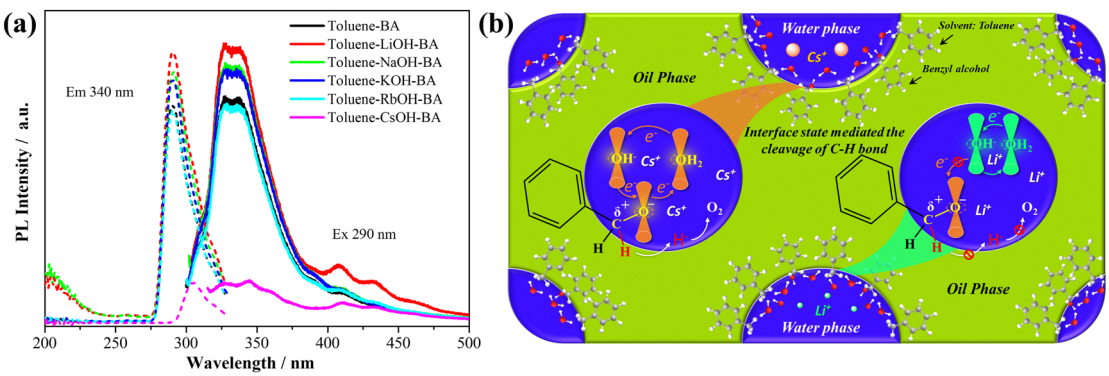

Fig. 5 Excitation and photoluminescence spectra (a) of the catalytic system (mixture of toluene, BA and MOH, M represented alkali metal cations, Li^+, Na^+, K^+, Rb^+ and Cs^+) of hydroxide and our proposed surface electronic states (SRSs) dominate the concerted electron and proton transfer mechanism (b).

interact with the C atom of $-CH_2$ to weaken the C–H bond. While the cleavage of the C–H bond was attributed to the formation of new surface electronic states due to the spatial overlap of p-orbitals of O atoms from the ternary system (M^+, H_2O and OH^-), which act as an alternative channel for concerted electron and proton transfer, thus facilitating the activation of O_2 and subsequent reaction kinetics. It is important to note that the unique oil–water biphasic interface serves as a prerequisite for electronic states through the spatial interaction of oxygen atom p-orbitals (Fig. 5b).

Reaction test and fluorescence spectrum demonstrate the presence of a water–hydroxyl–alkali metal cation complex ($(H_2O{\cdot}OH^-)M^+$), but there is insufficient evidence to determine its chemical structure. ^{1}H NMR spectroscopy provides direct evidence for this assignment. In order to improve the accuracy of H determination, we did not add additional water, since the source of H_2O only by absorption of H_2O in the air into the reaction system is sufficient to collect the information of the local hydrogen environments, except for CsOH which readily deliquesces to form amorphous or liquid mixtures. Depending on the presence or absence of MOH, the ^{1}H NMR spectrum in Fig. 6 shows two typical features with high resolution multiplets. In the absence of MOH, the ^{1}H spectrum of $PhCH_2OH$ alone is composed of three components (Fig. 6a and Fig. S6, ESI†): one set of resonance signals at the region between 7.2–7.5 ppm are aromatic hydrogens on the benzene ring, one resonance signal at *ca.* 4.60 ppm comes from $-CH_2-$ of $PHCH_2OH$, and the other one at *ca.* 5.82 ppm comes from the H of the alcohol hydroxyl group OH.

In general, the typical H chemical shift for single water molecules and OH^- species is located at *ca.* 4.8 ppm. However, only one resonance signal was observed: at *ca.* 6.26 ppm for Li^+, and within a narrow range of 5.62–5.89 ppm for other cations. This suggests that the signal originates from the H atom of the alcohol hydroxyl group, indicating that water and OH^- are coupled *via* a defined chemical structure. The integration area ratio of the 4.6 ppm peak ($-CH_2-$ of $PhCH_2OH$) to the 5.6–6.3 ppm region was estimated to be approximately 2 : 4 (Fig. S7–S10, ESI†). Excluding the contribution of excess water molecules surrounding the catalytic active site $(H_2O{\cdot}OH^-)M^+$, the complex composition is determined as $PhCH_2OH$ $(H_2O{\cdot}OH^-)M^+$ (Fig. 5b). The single peak center in the 5.6–6.3 ppm range confirms that all delocalized H atoms share the same chemical environment, exhibiting acidic properties.

As expected, the resonance signal at *ca.* 5.82 ppm—assigned to the H atom of the alcohol hydroxyl group—was not easily detected (Fig. 6a and Fig. S6–S10, ESI†). This suggests that the H^+ in the alcohol hydroxyl group of $PhCH_2OH$ is highly active (trace protons were detected at a chemical shift of 5.82 ppm, Fig. 6a and Fig. S6, ESI†). Consequently, it readily reacts with neighboring hydroxide ions, implying that the complex most likely exists as $PhCH_2O^-(H_2O{\cdot}OH_2)M^+$. This accounts for the estimated integration area ratio of ~2 : 4 between the 4.6 ppm peak ($-CH_2-$ of $PhCH_2OH$) and the 5.6–6.3 ppm region across all complexes with different alkali metal cations (Fig. S7–S10, ESI†). An exception is $PhCH_2O^-(H_2O{\cdot}OH_2)Cs^+$, which exhibits a remarkably low 4.6 ppm/5.62 ppm area ratio (2.00 : 10.68, Fig. S10, ESI†), attributed to the highly deliquescent nature of CsOH—introducing excessive water into the reaction system. Thus, ^{1}H NMR spectroscopy provides direct evidence that the intermediate species exists as $PhCH_2O^-(H_2O{\cdot}OH_2)M^+$ at the heterogeneous biphase interface.

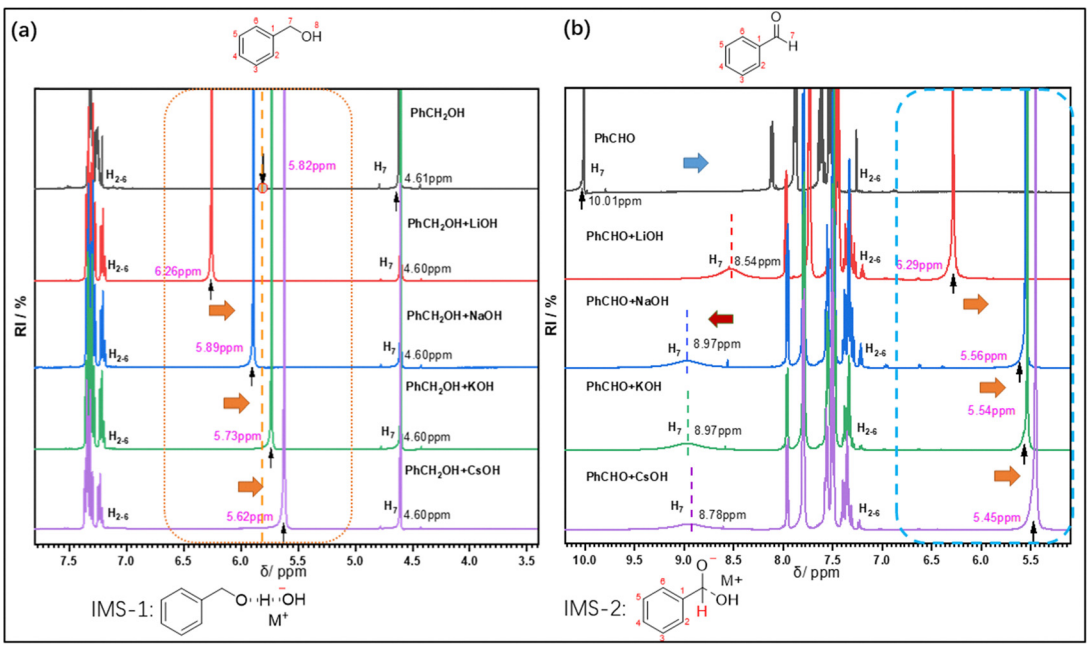

Fig. 6 ^{1}H NMR spectra to probe the intermediate species and the reaction mechanism of the oxidation of benzyl alcohol and benzaldehyde when using MOH (M = Li, Na, K, Cs) as a catalyst: (a) benzyl alcohol added MOH (M = Li, Na, K, Cs) as the catalyst; (b) benzaldehyde added MOH (M = Li, Na, K, Cs) as the catalyst.

Closer inspection revealed that the addition of LiOH and NaOH induced a low-field shift of the resonance signal at 5.82 ppm (to 6.26 ppm for LiOH and 5.89 ppm for NaOH), indicating a decrease in electron cloud density around the H nucleus. This suggests that both alkali metals exert a comparable electron-withdrawing inductive effect (Fig. S7 and S8, ESI†). Conversely, introducing KOH and CsOH caused a high-field shift of the 5.82 ppm signal (to 5.73 ppm for KOH and 5.62 ppm for CsOH), implying an increase in electron density around the H nucleus and suggesting an electron-donating inductive effect (Fig. S9 and S10, ESI†). Notably, the resonance signal at *ca.* 4.60 ppm remained unaffected, as expected, confirming the stability of the C–H bonds. Evidently, the presence of alkali metal cations with larger radii and greater hydrophobicity facilitates the enrichment of both $PhCH_2OH$ and O_2 reactants. This also modulates the electronic and geometric structure of the transition state, thereby altering the reaction pathways and enhancing the reaction kinetics.

To further investigate the inhibitory effect of alkali metal cations with large ionic radii on the aldehyde-to-acid reaction pathway, ^{1}H NMR spectroscopy was conducted to examine changes in the hydrogen nuclear chemical environment within benzaldehyde–MOH mixtures (Fig. 6b and Fig. S11–S15, ESI†). In the absence of MOH, the ^{1}H spectrum of PhCHO alone consists of two components (Fig. 6b and Fig. S11, ESI†): one set of resonance signals centered in the 7.2–8.0 ppm range corresponds to aromatic hydrogens on the benzene ring, and another signal centered at *ca.* 10.01 ppm originates from the –CHO hydrogen. However, upon introducing MOH, additional resonance signals centered in the 5.40–6.30 ppm range were observed (Fig. 6b and Fig. S12–S15, ESI†), indicating that the $(H_2O{\cdot}OH^-)\,M^+$ complex exhibits a similar electronic structure.

The key distinction lies in the significant alteration of the chemical environment for aldehyde-group hydrogen, shifting from a single narrow peak at 10.01 ppm to a broad peak that varies with alkali metal cations. LiOH induces the most pronounced chemical shift (from 10.01 to 8.54 ppm), with other cations affecting shifts in the order CsOH (8.78 ppm) > KOH (8.97 ppm) = NaOH (8.97 ppm). The half-peak width broadens in the sequence 0.85 ppm (LiOH) < 1.05 ppm (NaOH) < 1.15 ppm (KOH) < 1.30 ppm (CsOH), indicating enhanced electron delocalization around the hydrogen nucleus. Notably, when compared to $PhCH_2OH$ (Fig. 6a), the chemical shift variation of the complex, ranging from 6.29 to 5.45 ppm, is less pronounced for the same alkali metal cation (Fig. 6b), indicating that $(H_2O{\cdot}OH^-)M^+$ species exhibit characteristics of metastable intermediate molecules and analogous electronic states.

The most significant change occurs in the H atoms attached to the CHO functional group in BDA (Fig. 6b). Generally, Li^+ has the smallest ionic radius and highest charge density, leading to a strong electrostatic interaction with OH^-. This makes OH^- less prone to dissociate into free ions in solution, thereby reducing its nucleophilicity. Contrary to intuition, the chemical shift of H atoms bonded to the CHO group exhibits the largest chemical shift (*ca.* 1.47 ppm) with a very narrow half-peak width, suggesting that PhCHO interacts strongly with the $(H_2O{\cdot}OH^-)Li^+$ complex through the spatial overlap of p orbitals on C and O atoms. The most stable intermediate state is evidenced by the PL spectrum with the highest intensity (Fig. S16, ESI†). In contrast, for Na^+ and K^+—which have medium ionic radii and weaker affinity for OH^-—the smallest chemical shift (*ca.* 1.04 ppm) is observed (Fig. 6b), indicating weak electronic coupling between the C and O atoms (Fig. S16, ESI†). During the reaction, OH^- attacks the aldehyde group to form an alkoxide anion intermediate (IMS-2, Fig. 6b). The stabilizing effect of Na^+ and K^+ on this intermediate is relatively weak, facilitating subsequent proton transfer and disproportionation (*i.e.*, the Cannizzaro reaction). For Cs^+, the largest cation with the weakest affinity for OH^-, the PhCHO-$(H_2O{\cdot}OH^-)M^+$ complex cannot form (no PL signal, Fig. S16, ESI†), blocking subsequent proton and electron transfer and quenching the reaction. This likely explains the high selectivity of BA to BAD in the presence of Cs^+ (Fig. 4a). Thus, ^{1}H NMR not only provides direct evidence that the catalytic active site consists of $(H_2O{\cdot}OH^-)M^+$, but also explains why the reaction activity and selectivity trend depend on the ionic radius of alkali metal cations.

Conclusion

In summary, our metal-free catalytic system demonstrates exceptional performance in the selective oxidation of benzyl alcohol to benzaldehyde, with RbOH and CsOH catalysts enabling near-quantitative conversion (>99%) and high selectivity (>90%). Isotopic labeling experiments combined with advanced spectroscopic analyses—including UV-vis absorption, fluorescence spectroscopy, and ^{1}H NMR—unambiguously identify the water–hydroxyl–alkali metal cation complex $(H_2O{\cdot}OH^-)M^+$ at the biphasic interface as the active catalytic site. This complex generates surface electronic states (SESs) through the spatial overlap of p-orbitals from OH^- and H_2O at the subnano- and/or nanoscale interface, forming what we term p-band intermediate states (PBIS).[50,73,74] These states are exquisitely sensitive to subtle changes in the microenvironment around the active site, including the type of alkali metal cations, water content, solvent properties, and even the reactants themselves (benzyl alcohol and benzaldehyde). Indeed, these special surface states with π-character—operating *via* the Marcus inner-sphere electron transfer mechanism—act as a ligand bridge to facilitate electron–proton transfer at the nanoscale interface during the oxidation process, thereby enhancing the reaction kinetics significantly. Our findings not only elucidate the pivotal role of hydrated hydroxide complexes in selective alcohol oxidation but also offer new insights into electron–proton transfer mechanisms in homogeneous catalysis and at confined heterogeneous nano-interfaces. This work highlights the potential of designing metal-free catalytic systems for sustainable chemical synthesis.

Author contributions

K. Z. conceived the research concept and directed the project; B. P., W. Y. Z. and J. Y. D. conducted key experiments; B. P. and

K. Z. designed the experimental framework, and drafted the manuscript with support from C. J. X. and P. W.

Conflicts of interest

There are no conflicts to declare.

Data availability

All relevant data are within the manuscript and its Additional files.

Acknowledgements

This research was funded by the National Science Foundation of China (22172051, 21872053, and 21573074), the Joint laboratory for Low Carbon Energy and Chemical Processes of ECNU and Sinopec Research Institute of Petroleum Processing (Contract No. 36800000-24-ZC0607-0157), the Science and Technology Commission of Shanghai Municipality (19520711400) and the Research Funds of Happiness Flower ECNU (2020ST2203).

References

1 G. Zhan, Y. Hong, V. T. Mbah, J. Huang, A.-R. Ibrahim, M. Du and Q. Li, *Appl. Catal., A*, 2012, **439–440**, 179–186.
2 Y. Dai, X.-P. Wu, Y. Tang, Y. Yang, X.-Q. Gong and J. Fan, *Chem. Commun.*, 2016, **52**, 2827–2830.
3 Y. Yu, B. Lu, X. Wang, J. Zhao, X. Wang and Q. Cai, *Chem. Eng. J.*, 2010, **162**, 738–742.
4 L. Liu, X. Zhou, Y. Yan, J. Zhou, W. Zhang and X. Tai, *Polymers*, 2018, **10**, 1089.
5 F. M. Menger and C. Lee, *Tetrahedron Lett.*, 1981, **22**, 1655–1656.
6 M. Zhao, J. Li, E. Mano, Z. Song, D. M. Tschaen, E. J. Grabowski and P. J. Reider, *J. Org. Chem.*, 1999, **64**, 2564–2566.
7 H. Tohma, S. Takizawa, T. Maegawa and Y. Kita, *Angew. Chem., Int. Ed.*, 2000, **112**, 1362–1364.
8 R. Mazitschek, M. Mülbaier and A. Giannis, *Angew. Chem., Int. Ed.*, 2002, **41**, 4059–4061.
9 D. Ferri, C. Mondelli, F. Krumeich and A. Baiker, *J. Phys. Chem. B*, 2006, **110**, 22982–22986.
10 S. Hosokawa, Y. Hayashi, S. Imamura, K. Wada and M. Inoue, *Catal. Lett.*, 2009, **129**, 394–399.
11 A. Tanaka, K. Hashimoto and H. Kominami, *J. Am. Chem. Soc.*, 2012, **134**, 14526–14533.
12 F.-F. Wang, S. Shao, C.-L. Liu, C.-L. Xu, R.-Z. Yang and W.-S. Dong, *Chem. Eng. J.*, 2015, **264**, 336–343.
13 C. Zhou, Z. Guo, Y. Dai, X. Jia, H. Yu and Y. Yang, *Appl. Catal., B*, 2016, **181**, 118–126.
14 J. Sun, Y. Han, H. Fu, X. Qu, Z. Xu and S. Zheng, *Chem. Eng. J.*, 2017, **313**, 1–9.
15 C. Bianchi, F. Porta, L. Prati and M. Rossi, *Top. Catal.*, 2000, **13**, 231–236.
16 T. Mallat and A. Baiker, *Chem. Rev.*, 2004, **104**, 3037–3058.
17 B. N. Zope, D. D. Hibbitts, M. Neurock and R. J. Davis, *Science*, 2010, **330**, 74–78.
18 J. Li, D. Zhang, Y. Chi and C. Hu, *Polyoxometalates*, 2022, **1**, 9140012.
19 S.-M. Zhang, Y. Wang, Y.-Y. Ma, Z.-B. Li, J. Du and Z.-G. Han, *Inorg. Chem.*, 2022, **61**, 20596–20607.
20 Q. Gu, X.-L. Zhao, M. Meng, Z. Shao, Q. Zheng and W. Xuan, *Chin. Chem. Lett.*, 2023, **34**, 107444.
21 K. Qin, D. Zang and Y. Wei, *Chin. Chem. Lett.*, 2023, **34**, 107999.
22 Y. Wang, Z.-X. Liu, X.-P. Zhao, Y.-Y. Ma, S.-M. Zhang, W.-J. Cui, J. Du and Z.-G. Han, *Chin. J. Struct. Chem.*, 2023, **42**, 100011.
23 D. Hacıefendioğlu and A. Tuncel, *Catal. Sci. Technol.*, 2024, **14**, 6524–6536.
24 Y. Wang, Q. Liu, Y.-Y. Ma, Z.-X. Liu, Y.-N. Zhang, Y.-S. Wang, J. Du and Z.-G. Han, *Mol. Catal.*, 2024, **569**, 114579.
25 M. S. Ide and R. J. Davis, *Acc. Chem. Res.*, 2014, **47**, 825–833.
26 S. Carrettin, P. McMorn, P. Johnston, K. Griffin and G. J. Hutchings, *Chem. Commun.*, 2002, 696–697.
27 W. Ketchie, Y. Fang, M. Wong, M. Murayama and R. Davis, *J. Catal.*, 2007, **250**, 94–101.
28 Y. Ryabenkova, P. J. Miedziak, N. F. Dummer, S. H. Taylor, N. Dimitratos, D. J. Willock, D. Bethell, D. W. Knight and G. J. Hutchings, *Top. Catal.*, 2012, **55**, 1283–1288.
29 M. B. Griffin, A. A. Rodriguez, M. M. Montemore, J. R. Monnier, C. T. Williams and J. W. Medlin, *J. Catal.*, 2013, **307**, 111–120.
30 P. Xin, J. Li, Y. Xiong, X. Wu, J. Dong, W. Chen, Y. Wang, L. Gu, J. Luo, H. Rong, C. Chen, Q. Peng, D. Wang and Y. Li, *Angew. Chem., Int. Ed.*, 2018, **57**, 4642–4646.
31 S. Biella, L. Prati and M. Rossi, *Inorg. Chim. Acta*, 2003, **349**, 253–257.
32 S. Carrettin, P. McMorn, P. Johnston, K. Griffin, C. J. Kiely and G. J. Hutchings, *Phys. Chem. Chem. Phys.*, 2003, **5**, 1329–1336.
33 H. Liu, Y. Liu, Y. Li, Z. Tang and H. Jiang, *J. Phys. Chem. C*, 2010, **114**, 13362–13369.
34 D. D. Hibbitts and M. Neurock, *J. Catal.*, 2013, **299**, 261–271.
35 C. Shang and Z.-P. Liu, *J. Am. Chem. Soc.*, 2011, **133**, 9938–9947.
36 J. Wang, C. Liu, J. Yuan and A. Lei, *New J. Chem.*, 2013, **37**, 1700.
37 Z.-F. Yuan, W.-N. Zhao, Z.-P. Liu and B.-Q. Xu, *J. Catal.*, 2017, **353**, 37–43.
38 G. M. Mullen, E. J. Evans, I. Sabzevari, B. E. Long, K. Alhazmi, B. D. Chandler and C. B. Mullins, *ACS Catal.*, 2017, **7**, 1216–1226.
39 L. Zhang, J. Liu, F. Zhang and X.-M. Zhang, *J. Catal.*, 2017, **354**, 78–83.
40 Q. Gu, P. Sautet and C. Michel, *ACS Catal.*, 2018, **8**, 11716–11721.
41 D. Muñoz-Santiburcio, M. Farnesi Camellone and D. Marx, *Angew. Chem., Int. Ed.*, 2018, **57**, 3327–3331.
42 C.-R. Chang, X.-F. Yang, B. Long and J. Li, *ACS Catal.*, 2013, **3**, 1693–1699.

43 H.-V. Tran, H. A. Doan, B. D. Chandler and L. C. Grabow, *Curr. Opin. Chem. Eng.*, 2016, **13**, 100–108.
44 Q. Wei, C. Yu, X. Song, Y. Zhong, L. Ni, Y. Ren, W. Guo, J. Yu and J. Qiu, *J. Am. Chem. Soc.*, 2021, **143**, 6071–6078.
45 J. Zhou, T. Yang, B. Peng, B. Shan, M. Ding and K. Zhang, *ACS Phys. Chem. Au*, 2022, **2**, 47–58.
46 T.-Q. Yang, X.-D. Hu, B.-Q. Shan, B. Peng, J.-F. Zhou and K. Zhang, *Nanoscale*, 2021, **13**, 15058–15066.
47 B. Peng, L.-X. Zheng, P.-Y. Wang, J.-F. Zhou, M. Ding, H.-D. Sun, B.-Q. Shan and K. Zhang, *Front. Chem.*, 2021, **9**, 756993.
48 T. Yang, J. Zhou, B. Shan, L. Li, C. Zhu, C. Ma, H. Gao, G. Chen, K. Zhang and P. Wu, *Macromol. Rapid Commun.*, 2022, **43**, 2100720.
49 B. Peng and K. Zhang, *Chem. – Eur. J.*, 2025, **31**, e202500499.
50 B. Peng, K. Zhang and M.-Y. He, *Langmuir*, 2023, **39**, 13409–13419.
51 B. Peng, J.-F. Zhou, M. Ding, B.-Q. Shan, T. Chen and K. Zhang, *Sci. Technol. Adv. Mater.*, 2023, **24**, 2210723.
52 T. Yang, B. Shan, F. Huang, S. Yang, B. Peng, E. Yuan, P. Wu and K. Zhang, *Commun. Chem.*, 2019, **2**, 1–11.
53 M. He, K. Zhang, Y. Guan, Y. Sun and B. Han, *Natl. Sci. Rev.*, 2023, **10**, nwad046.
54 J. Ewles, *Nature*, 1930, **125**, 706–707.
55 K. Przibram, *Nature*, 1958, **182**, 520.
56 X.-D. Hu, B.-Q. Shan, R. Tao, T.-Q. Yang and K. Zhang, *J. Phys. Chem. C*, 2021, **125**, 2446–2453.
57 B. Q. Shan, J. F. Zhou, M. Ding, X. D. Hu and K. Zhang, *Phys. Chem. Chem. Phys.*, 2021, **23**, 12950–12957.
58 R. Tao, B.-Q. Shan, H.-D. Sun, M. Ding, Q.-S. Xue, J.-G. Jiang, P. Wu and K. Zhang, *J. Phys. Chem. C*, 2021, **125**, 13304–13312.
59 M. Ding, B.-Q. Shan, B. Peng, J.-F. Zhou and K. Zhang, *Phys. Chem. Chem. Phys.*, 2022, **24**, 7923–7936.
60 P.-Y. Wang, J.-F. Zhou, H. Chen, B. Peng and K. Zhang, *JACS Au*, 2022, **2**, 1457–1471.
61 L.-X. Zheng, B. Peng, J.-F. Zhou, B.-Q. Shan, Q.-S. Xue and K. Zhang, *Microporous Mesoporous Mater.*, 2022, **342**, 112140.
62 M. Ding, B. Peng, J. Zhou, H. Chen, Y.-S. Chen, E.-H. Yuan, B. Albela, L. Bonneviot, P. Wu and K. Zhang, *Catal. Sci. Technol.*, 2023, **13**, 2001–2009.
63 B. Peng, B. Shan, K. Lam and K. Zhang, *ChemCatChem*, 2024, **17**, e202401505.
64 J.-F. Zhou, B. Peng, M. Ding, B.-Q. Shan, Y.-S. Zhu, L. Bonneviot, P. Wu and K. Zhang, *Phys. Chem. Chem. Phys.*, 2024, **26**, 18854–18864.
65 Y. Gao and X. C. Zeng, *ACS Catal.*, 2012, **2**, 2614–2621.
66 C. Yu, L. Fan, J. Yang, Y. Shan and J. Qiu, *Chem. – Eur. J.*, 2013, **19**, 16192–16195.
67 L. Ni, C. Yu, Q. Wei, J. Chang and J. Qiu, *Green Chem.*, 2020, **22**, 5711–5721.
68 K. S. Han, Z. Yu, H. Wang, P. C. Redfern, L. Ma, L. Cheng, Y. Chen, J. Z. Hu, L. A. Curtiss, K. Xu, V. Murugesan and K. T. Mueller, *J. Phys. Chem. B*, 2020, **124**, 5284–5291.
69 M. Han, R. Zhang, A. A. Gewirth and R. M. Espinosa-Marzal, *Nano Lett.*, 2021, **21**, 2304–2309.
70 G. Horwitz, E. Härk, P. Y. Steinberg, L. P. Cavalcanti, S. Risse and H. R. Corti, *ACS Nano*, 2021, **15**, 11564–11572.
71 N. H. C. Lewis, B. Dereka, Y. Zhang, E. J. Maginn and A. Tokmakoff, *J. Phys. Chem. B*, 2022, **126**, 5305–5319.
72 S. Subbiah, S. P. Simeonov, J. M. S. S. Esperança, L. P. N. Rebelo and C. A. M. Afonso, *Green Chem.*, 2013, **15**, 2849.
73 B. Peng, K. Zhang, Y. Sun, B. Han and M. He, *J. Am. Chem. Soc.*, 2025, **147**, 13083–13100.
74 B. Peng, Y. Zhu, M. Ding, B. Albela, L. Bonneviot and K. Zhang, *J. Phys. Chem. Lett.*, 2025, **16**, 6116–6124.